From band tailing to impurity-band formation and discussion of localization in doped semiconductors: A multiple-scattering approach

J. Serre and A. Ghazali

Groupe de Physique des Solides de l'Ecole Normale Supérieure, Laboratoire associé au Centre National de la Recherche Scientifique, Université Paris VII, Tour 23, 2 place Jussieu, F-75221 Paris 5, France

(Received 23 December 1982)

Klauder's best multiple-scattering approximation which allows the use of a realistic interaction potential and in which electron-electron interactions may be incorporated is shown to constitute a sound basis for the study of the electronic structure of doped semiconductors. The implementation of this formalism requires the solution of a self-consistent set of nonlinear integral equations. This has been done numerically over a large impurity-concentration range. We have thus shown that as the concentration decreases, the band tail gradually splits off from the main band, giving an impurity band. Spectral-density analysis allows one to distinguish between localized and extended states. Compensation effects have also been analyzed. Finally, our results are discussed and compared with various experiments.

I. INTRODUCTION

Experimentally the most studied disordered systems are certainly doped semiconductors (DSC's). The disorder here arises from the random position of impurities and also from the chemical nature of these impurities (donors or acceptors). It has been well established that DSC's undergo a nonmetal-to-metal transition beyond a critical impurity concentration.[1] Theoretically the nature of the metal-nonmetal transition (M-NMT) is still not completely elucidated. The question is whether the M-NMT occurs at the closing of a density-of-states gap due to Coulomb interactions within the system (correlation gap) or when the Fermi level crosses a mobility gap within a continuum of states. In other words, one has to evaluate the respective roles of disorder and of electron correlations in this transition. Recently, the localization in disordered systems has been the subject of a large number of theoretical studies[2] dealing mainly with transport properties. It has by now become evident both experimentally[3] and theoretically[2] that disorder and correlation effects are both important in the understanding of the problem of localization. From a different point of view, in order to bring a better understanding of the M-NMT in DSC's and of the nature of the localization in these systems, we propose here to use a multiple-scattering method to study the electronic structure of DSC's as a function of the doping level and of compensation taking into account electron-electron interaction effects.

Since the first studies on the electronic structure of the impurity band by Klauder[4] and Matsubara and Toyozawa[5] much work has been devoted to disordered systems especially binary alloys. Most of these studies use the coherent-potential approximation (CPA) within the framework of the tight-binding model. The CPA is known to be the best single-site approximation[6]; however, its practical implementation involves the use of a somewhat unphysical δ-function potential for the electron-impurity interaction. With such a potential the calculations are considerably simplified but one obtains a wave-vector-independent self-energy $\Sigma(E)$. Already in 1961, Klauder[4] proposed a multiple-scattering formalism which enables one to account for a realistic interaction potential, eventually self-consistent. However, Klauder's theory does not include the multiple-occupancy corrections.[6,7] We will show that in our system these corrections are unlikely to modify qualitatively our conclusions. Therefore, we have found it of interest to use this theory with a realistic potential. This formalism has been numerically implemented; to the best of our knowledge, this has never previously been done. It provides us with a novel description[8] of the electronic structure of the M-NMT in DSC's which appears quite reasonable. We have thus shown that at high impurity concentration, the conduction (valence) band presents a tail extending in the band gap. As the concentration is lowered, an erosion appears between the main body and the tail of the band. This erosion becomes more pronounced and leads finally to a separate impurity band.

The aim of this paper is (i) to give a detailed description of our multiple-scattering treatment of electron-impurity interaction in DSC's, taking into account electron-electron interaction effects in an approximate way, (ii) to present an analysis of the spectral density as a function of concentration and energy that enables us to distinguish localized states from extended ones, and (iii) to show the sizable effects of compensation on the electronic structure and on the nature of transition. The paper is organized as follows: In Sec. II, we present and discuss electron-electron and electron-impurity interactions. In Sec. III, Klauder's multiple-scattering formalism is analyzed and the multiple-occupancy corrections are discussed. Klauder's formalism is expressed by a self-consistent set of nonlinear integral equations the numerical solution of which is presented in Sec. IV. The results of calculations applied to our DSC model are detailed in the following sections: the density of states and the formation of the impurity band in Sec. V, the spectral density and the discussion of the localization in Sec. VI, and the compensation effects in Sec. VII. Lastly, these results are discussed and compared with experiment in Sec. VIII.

II. ELECTRON-ELECTRON AND ELECTRON-IMPURITY INTERACTIONS

We consider a DSC in which the impurities (donors and acceptors) are assumed to be fixed and randomly distributed throughout the crystal with the average concentration N_D. Concentration fluctuations around the average concentration will be neglected here but may be included in the same way as in a previous work.[9] It is known that potential fluctuations generally yield an extension of the density of states beyond the band edges determined with a uniform concentration. However, the fraction of states involved in this process is relatively small.[9]

In the framework of the effective-mass approximation, the Hamiltonian of the system reads as follows:

$$\mathcal{H}=-\sum_i \frac{\hbar^2\nabla_i^2}{2m^*}+\tfrac{1}{2}\sum_{\substack{i,j\\ i\neq j}}\frac{e^2}{\kappa\,|\,\vec{r}_i-\vec{r}_j\,|}-\sum_{i,j}\frac{e^2}{\kappa\,|\,\vec{r}_i-\vec{R}_j\,|}+\tfrac{1}{2}\sum_{\substack{i,j\\ i\neq j}}\frac{e^2}{\kappa\,|\,\vec{R}_i-\vec{R}_j\,|}\ . \tag{1}$$

Here m^* is the electron effective mass, κ the dielectric constant, and $\vec{r}$'s and $\vec{R}$'s denote the electron and impurity positions, respectively. The first term in (1) is the Hamiltonian of the pure material. The second, third, and fourth terms represent electron-electron, electron-impurity, and impurity-impurity interactions, respectively. It is known that a standard way to describe the one-electron properties of an interacting electron system is to use the one-electron Green function $G(\vec{k},E)$, where $\vec{k}$ and E are, respectively, the wave vector and energy of the quasiparticle.[10] This Green function obeys the Dyson equation

$$G(\vec{k},E)=[E-\epsilon_k-\Sigma(\vec{k},E)]^{-1}\ .$$

Here ϵ_k is the electron eigenenergy of the noninteracting system and $\Sigma(\vec{k},E)$ the electron self-energy. For the sake of simplicity, a single conduction (valence) band with the parabolic dispersion law $\epsilon_k=\hbar^2k^2/2m^*$ is assumed, but it is clear that the formalism used in this work may in principle, include more complex band structures. On the other hand, the electron self-energy is the sum of the exchange-correlation (xc) and electron-impurity (ei) contributions, i.e., $\Sigma(\vec{k},E)=\Sigma_{xc}(\vec{k},E)+\Sigma_{ei}(\vec{k},E)$, which result from the second and third terms in (1), respectively. To evaluate the Green function, we need to know these contributions. They are calculated as the sums of a perturbation series in electron-electron and electron-impurity interactions, respectively. It is understood that the latter interactions are averaged over all possible impurity configurations in the Kohn-Luttinger sense.[11] In the perturbation series, the first-order Coulomb terms cancel each other due to the overall electrical neutrality. Wolff[12] has shown that this result remains exact even when the Coulomb interactions are screened.

In the following sections, we show how the mathematical expression for $\Sigma_{ei}(\vec{k},E)$ is obtained and evaluated numerically. As for $\Sigma_{xc}(\vec{k},E)$, there have been a large number of studies which show that it depends only very slightly on k even beyond the Fermi wave vector k_F.[13,14]

Moreover, in the energy range of interest, the energy dependence of Σ_{xc} is also negligible.[15] Σ_{xc} has been approximated furthermore by its exchange part taken at the Fermi level $\Sigma_x=-(e^2/\kappa)(3N/\pi)^{1/3}$ where N is the electron (hole) concentration. This is a high-density approximation consistent with the chosen effective potential which we will now consider.

Owing to electron-electron interactions, any charge in the system will be screened.[16] Therefore, the electron-impurity potential $v(\vec{r})$ which enters the expression of Σ_{ei} (see Sec. III) will also be screened. To include the screening effect, we will content ourselves by taking the Thomas-Fermi (TF) effective potential $v(\vec{r})=\pm(e^2/\kappa r)\exp(-q_s r)$ where q_s is the inverse screening length. The strength and the range of this potential depend on the electron (hole) concentration N through the relation

$$q_s^2=2(e^2/\kappa)(2m^*/\hbar^2)(3N/\pi)^{1/3}\ .$$

The total self-energy and the Green function which we will consider in Sec. III depend on Σ_{ei} and on Σ_{xc}. Σ_{ei}, in turn, depends on the effective potential. Our approximation for the effective potential, i.e., the TF one, is certainly correct at high concentrations. It is less accurate at intermediate concentrations and even nonvalid at low concentrations for which a separate impurity band appears. In the latter case, electrons are localized but a potential weakening does exist because of the electron polarization.[17] However, the TF potential can account qualitatively for such a weakening. It should be noted that TF potential has the right limit at vanishing concentrations, i.e., the bare Coulomb potential. In fact, it should be necessary to have a completely self-consistent effective potential in order to describe quantitatively electron-impurity and electron-electron interactions at any concentrations. The local density-functional method[14,18] seems to be a good tool to obtain such an effective potential. This is an elaborate scheme that we shall not consider at this stage. Meanwhile, it is hoped that our approximations outlined above are reasonable enough to help to describe at least qualitatively how the band structure changes with doping level. Our results would seem to confirm that this is indeed the case.

III. MULTIPLE SCATTERING

Klauder's best multiple-scattering approximation[4] [the fifth one, Eqs. (75)—(77) of his paper] has been used. This approximation is expressed in the momentum representation by a self-consistent set of nonlinear integral equations which we rewrite as follows (the exchange-correlation contribution to the self-energy has been incorporated):

$$K(\vec{k},\vec{q};E)=\frac{1}{(2\pi)^3}\int d^3q'v(\vec{q}\,'-\vec{q})G(\vec{k}+\vec{q}\,';E)\times[N_D v(-\vec{q}\,')+K(\vec{k},\vec{q}\,';E)]\ , \tag{2a}$$

$$\Sigma_{ei}(\vec{k},E)\equiv K(\vec{k},\vec{q}=0;E)\ , \tag{2b}$$

$$\Sigma(\vec{k},E)=\Sigma_{ei}(\vec{k},E)+\Sigma_{xc}(\vec{k},E)\ , \tag{2c}$$

$$G(\vec{k},E)=[E-\epsilon_k-\Sigma(\vec{k},E)]^{-1}\ . \tag{2d}$$

Here $v(\vec{q})$ is the Fourier transform of impurity potential, E the electron energy, ϵ_k the eigenenergy of unperturbed system, and $G(\vec{k},E)$ the average Green function of the perturbed system. The vertex function $K(\vec{k},\vec{q};E)$ leads to the self-energy Σ_{ei} through (2b). Note that functions G, K, and Σ, are generally complex.

In Appendix A, it is shown how the best single-site Klauder's approximation [Eqs. (2a)—(2d)] may be derived diagrammatically. It is also shown that this approximation accounts for scattering from a given site to all orders in v and to all orders in N_D through an effective medium.

Once the Green function is determined, one may calculate the spectral density as follows:

$$A(\vec{k},E)=\mp\left[\frac{1}{\pi}\right]\mathrm{Im}G(\vec{k},E\pm i0)\ , \tag{3}$$

which is the average probability that an electron having energy E is in the state $|\vec{k}\rangle$, and the density of states (DOS) per unit energy and unit volume,

$$D(E)=\left[\frac{1}{\Omega}\right]\mathrm{Tr}A(\vec{k},E)\ , \tag{4}$$

where Ω is the volume and Tr means the sum over the $\vec{k}$'s and the spin states. In the following we have (arbitrarily) taken a twofold spin degeneracy in order to recover the standard DOS for a free-electron gas. A method to solve the set of Eqs. (2a)—(2d) will be displayed in Sec. IV.

It can be shown that Klauder's theory neglects the so-called occupancy corrections.[6] These corrections are easily understood if one considers for instance, two-impurity diagrams (f) and (g) in Fig. 9. Diagram (f) occurs in the summation leading to Dyson equation [Eq. (A3)], while diagram (g) comes out when the bare propagator G_0 in Eq. (A1) is replaced by the renormalized propagator G. In both cases, one has to make sure that the impurity i is different from impurity j; otherwise, one obtains an unphysical diagram similar to (h) in Fig. 9 which is proportional to N_D^2 and thus does not have to be taken into account.

At present, we find no straightforward way to include these corrections in Klauder's formalism. However, they may be easily included within the tight-binding Hamiltonian with a δ-function site potential.[6] In this case, with the multiple-occupancy corrections, the fourth and fifth Klauder's approximations yield the average T-matrix approximation and the coherent-potential approximation (CPA), respectively. In order to assess the importance of these corrections in our problem we have calculated (in the tight-binding model with zero-range potential) the DOS as a function of impurity concentration and of potential strength both with and without multiple-occupancy corrections. This is given in Appendix B. With δ-function potential and for usual impurity concentrations in DSC's (typically the fraction of impurities is of the order of 10^{-6} to 10^{-4}) the conclusions are the following: (i) At given concentration, the critical potential for the opening of the gap is the same in both approximations, (ii) the impurity band when it exists is centered in both approximations at the value given by the Koster-Slater model whatever the potential strength, and (iii) the impurity band broadens when multiple-occupancy corrections are neglected. Therefore, these corrections do not seem essential in the concentration range of interest at least for a δ-function potential. Although these conclusions do not directly apply to the finite extension-potential case, it is certainly interesting to use Klauder's formalism because unlike the tight-binding CPA it does enable us to include a realistic and eventually self-consistent potential.

IV. IMPLEMENTATION OF THE MODEL

In order to obtain the self-energy $\Sigma(\vec{k},E)$ and the Green function $G(\vec{k},E)$ which characterize our system, Eqs. (2a)—(2d) have to be solved at different concentrations N_D, different energies E, and different wave vectors $\vec{k}$. Equation (2a) resembles a second-kind Fredholm integral equation but it is nonlinear because G depends explicitly on K through (2d) and (2b). It should be noted that to obtain Σ_{ei} at given $\vec{k}$, it is necessary to calculate the function K at $\vec{k}$ but also at all values of $\vec{q}$. To our knowledge these calculations have only been performed so far for the δ-function potential, in which case the integral equation (2a) reduces to an algebraic equation for Σ. This has been done by Klauder[4] for a one-dimensional system. This model was taken up again by Yonezawa[19] but in the three-dimensional case, having recourse to an *ad hoc* cutoff in $G(\vec{k})$ in order to avoid divergence.

In the present work, we are dealing with a three-dimensional system and a wave-vector-dependent scattering potential $v(\vec{q})=-4\pi e^2/\kappa(q^2+q_s^2)$. We have then to solve a genuine three-dimensional set of integral equations. Our system is invariant under rotation because the impurity distribution is assumed to be macroscopically isotropic and also because ϵ_k does not depend here on the direction of $\vec{k}$. Therefore, the Green function $G(\vec{k},E)$ and the self-energy $\Sigma(\vec{k},E)$ depend only on $|\vec{k}|$ while the vertex function $K(\vec{k},\vec{q};E)$ depends only on $|\vec{k}|$, $|\vec{q}|$, and the angle they form. It follows that in spherical coordinates the integration over ϕ can be performed analytically.

Now the set of equations has to be solved numerically. At first glance the simplest way to do it is to use an iterative process: Given a starting function $G(\vec{k},E)$ and setting, for instance, $K\equiv 0$ in the right-hand member of (2a), one then obtains new functions $K(\vec{k},\vec{q};E)$, $\Sigma(\vec{k},E)$, and $G(\vec{k},E)$. These functions are again introduced in Eq. (2a) until convergence is reached. However, one encounters two major difficulties in this method which will now be pointed out.

(i) The iterative process described above is equivalent to a standard perturbation expansion and like the latter, it is convergent only if the perturbing potential is weak enough compared to the characteristic energies of the system. This may easily be seen by writing formally Eq. (2a) under the form

$$K=N_D v G v+vGK\ , \tag{5a}$$

which gives the solution

$$K=N_D(1-vG)^{-1}vGv\ . \tag{5b}$$

It is clear that as $|vG|$ becomes comparable to one, the series expansion of Eq. (5b) in powers of vG becomes slowly convergent or even divergent.[20] Such situations occur

effectively for low enough concentrations (strong potential) and in energy ranges around band edges. The divergence of the process is such that even if the input functions K and G are very close to the solutions, iterated functions deviate more and more from the starting ones. This is evidence of the failure of this iterative process but it does not mean that Eq. (5b) has no solution.

(ii) The functions K, Σ, and G being complex, it is easy to see by taking real and imaginary parts of (2a) that if K is a solution its complex conjugate is also a solution. The same is true for Σ and G. More precisely,

$$\mathrm{Im}\Sigma(E-i0)=-\mathrm{Im}\Sigma(E+i0)$$

and similarly for G and K. Hence one has mathematically two limit solutions for real energies when $\mathrm{Im}\Sigma\neq 0$, i.e., two solutions for the DOS, $D^{+}(E)=D(E)$ [Eq. (4)] and $D^{-}(E)=-D(E)$; only the former has a physical meaning. One may then expect that convergence is not ensured in the neighborhood of band edges. The latter appear as singular values of energy. The formation of an impurity band is an example of the general problem of bifurcation which arises in systems governed by nonlinear equations.[21] In our system the band edges are nothing but bifurcation points.[8]

Another method is therefore needed to solve Eqs. (2a)—(2d). The basic ideas of the method we put forward are the following. (i) Linearize Eq. (2a) by taking for G a K-independent, fixed function, e.g., that obtained at high energy. The integral equation (2a) is then discretized according to the relevant values of $\vec{q}\,'$ leading to a set of complex linear equations which is solved exactly by a numerical method. (ii) The solution K thus obtained leads via Eqs. (2b)—(2d) to a new function G which in turn is introduced in Eq. (2a) and the process (i) is repeated until a self-consistent solution is reached. This method is free of the divergence problems encountered when solving Eq. (5b) by the simple iterative technique because in step (i) above, for a given G, Eq. (5b) is transformed into a set of linear equations which is exactly solved and no iteration is used.

In fact, both real and imaginary parts of the integrand in (2a) exhibit strong $\vec{q}\,'$ dependences which are essentially due to G. This makes integration calculations rather lengthy especially if a reasonable accuracy is desired. A substantial improvement of the method is to try to minimize those parts of calculations in which these rapid variations occur. To this end, it is useful to make the following transformations.

Firstly, the variable changes $(\vec{k}+\vec{q})\rightarrow\vec{q}$ and $(\vec{k}+\vec{q}\,')\rightarrow\vec{q}\,'$ lead to a function which we still denote by K that obeys the integral equation in which G depends only on $|\vec{q}\,'|$:

$$K(\vec{k},\vec{q};E)=\frac{1}{(2\pi)^3}\int d^3q'v(\vec{q}\,'-\vec{q})G(\vec{q}\,',E)\times[N_D v(\vec{k}-\vec{q}\,')+K(\vec{k},\vec{q}\,';E)]\ , \tag{6a}$$

with

$$\Sigma_{ei}(\vec{k},E)\equiv K(\vec{k},\vec{k};E)\ . \tag{6b}$$

Secondly, the function change,

$$U(\vec{k},\vec{q};E)=K(\vec{k},\vec{q};E)+N_D v(\vec{k}-\vec{q})\ , \tag{7}$$

leads to the integral equation for the function U as follows:

$$U(\vec{k},\vec{q};E)=N_D v(\vec{k}-\vec{q})+\frac{1}{(2\pi)^3}\int d^3q'v(\vec{q}\,'-\vec{q})\times G(\vec{q}\,')U(\vec{k},\vec{q}\,';E)\ , \tag{8a}$$

with

$$\Sigma_{ei}(\vec{k},E)\equiv U(\vec{k},\vec{k};E)-N_D v(0)\ , \tag{8b}$$

$$\Sigma(\vec{k},E)=\Sigma_{ei}(\vec{k},E)+\Sigma_{xc}(\vec{k},E)\ , \tag{8c}$$

$$G(\vec{k},E)=[E-\epsilon_k-\Sigma(\vec{k},E)]^{-1}\ . \tag{8d}$$

Formally, Eq. (8a) may be written as follows:

$$U=N_D v+vGU\ . \tag{9a}$$

It leads to a linearized equation in U to be solved exactly:

$$(1-vG)U=N_D v\ . \tag{9b}$$

It is precisely this equation we have solved numerically by the method described above. Here the operator $(1-vG)$ does not depend on $\vec{k}$ in contrast to the corresponding term in (5b) and numerical calculations are performed once and for all when $\vec{k}$ is varied. Moreover, the right-hand member of Eq. (9b) is simply proportional to the effective potential while that of Eq. (5b) requires a cumbersome integration which leads to less accurate results. Let us emphasize that the solution is independent of the input function G.

Finally, as noted above, in the complex energy plane $(E\pm iE')$, the imaginary parts of G, U, and Σ, when finite, are discontinuous functions on the real axis. It is often necessary, especially around band edges to perform calculations at complex energies and then extrapolate for $E'=0$. For a given set of parameters (N_D, E, and E') the solutions $G(\vec{k},E)$ and $K(\vec{k},\vec{q};E)$ are obtained after only a few iterations ($\lesssim 10$). In the following sections, we present and discuss our results and compare them with experimental data.

V. DENSITY OF STATES

The set of integral equations (8a)—(8d) is solved for different concentrations N_D over 5 orders of magnitude covering in particular the M-NMT concentration range. Then at given concentration, calculations are made for different energies around the bottom of conduction band (CB) [or respectively, the top of valence band (VB)]. Lastly, at given concentration and energy, the set of equations is solved for an appropriate sampling of vectors $\vec{k}$ and $\vec{q}$.

In the following, energies, lengths, DOS's, and concentrations are, respectively, given in units of effective rydberg $R=m^{*}e^4/2\hbar^2\kappa^2$, of effective Bohr radius $a_0=\hbar^2\kappa/m^{*}e^2$, states per Ra_0^3, and $(\pi/3)(4a_0)^{-3}$. The DOS's thus obtained are plotted in Fig. 1 as functions of energy for different impurity concentrations[22] N_D. As can

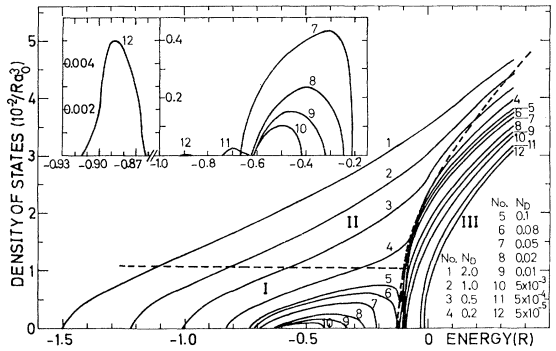

FIG. 1. DOS's as functions of energy for different impurity concentrations N_D. The insets show the impurity-band DOS's (enlarged scales) for several concentrations. Regions I, II, and III delimited by dashed lines are domains of existence of localized, hybrid, and extended states, respectively (see Sec. VI).

be seen, at high concentrations the CB shows a tail extending towards low energies. A concavity change in the DOS appears with the beginning of the band tail. As N_D decreases, the latter shrinks and the concavity change leads finally to the formation of an impurity band (IB) split off from the CB by an energy gap. The latter appears at $N_D \simeq 0.1$ (i.e., $N_D^{1/3} a_0 \simeq 0.12$ in usual units). The gap widens out as N_D decreases (see Fig. 2) and tends towards the hydrogenic limit ($1R$). This is noteworthy because the states of the unperturbed system are those of free electrons with positive energies. This result attests to the value of the present multiple-scattering method. At very low concentrations, the CB DOS is found to be practically equal to that of free-electron gas [$\sqrt{E}/(2\pi^2)$] as expected. Let us point out that our method leads without an *a priori* hypothesis to two different kinds of states (IB and perturbed CB ones).

Let us now set out the main features of IB. (i) Its DOS is asymmetric. It falls off on its high-energy side while it decreases smoothly on its low-energy side and vanishes at a definite energy. This asymmetry has been obtained by other authors using various methods: Matsubara and Toyozawa[5] by using a diagrammatic method in site representation for the tight-binding Hamiltonian, Yonezawa[19] whose model has been outlined above (see Sec. IV), Gaspard and Cyrot-Lackmann[23] by using the tight-binding model and moment expansion of the Green function. It should be noted, however, that the IB asymmetry becomes less apparent as the IB moves off from the CB (see Fig. 1). (ii) We have checked for all explored concentrations that the integrated DOS over the IB when it exists is equal (to within a few percent) to the impurity concentration as it should be. Such a property is satisfied only if no spin degeneracy is assumed over the IB spectrum. This sum rule is one of the fundamental properties which follow from the analyticity of Green function. It has been demonstrated in various models.[24] It can easily be understood by considering the spectral density operator[25] which leads under certain conditions to the sum rule for the spectral density defined by Eq. (3):

$$\int_{E_1}^{E_2} A(\vec{k},E)dE = 1 ,$$

where E_1 and E_2 are the IB edges. It is clear that if in Eq. (4) the summation over spin variables is omitted, the DOS obeys the sum rule[26]

$$\int_{E_1}^{E_2} D(E)dE = N_D .$$

This sum rule implies that states forming the IB or the band tail are extracted from the main band because the total number of states must be invariant. One then would expect a crossing of the perturbed and unperturbed DOS's. Such crossing points do not appear in Fig. 1; they are pushed away at higher energy because our perturbed CB's are shifted towards low energies as a result of the exchange-correlation term. Finally, it should be noted that other analytic properties of the Green function as defined by Nakanishi *et al.*[24] are satisfied in the present model.

Before concluding this section, it is interesting to compare the DOS's obtained by scattering calculations to all orders in potential on a site (present calculations) and those obtained in the high-density approximation (see Appendix A). This is illustrated in Fig. 3. At high energies, both approximations lead to the same results. This confirms that in this energy range multiple-scattering effects are negligible. In contrast, at low energies, in the high-density approximation (dashed curves) there is no concavity change in the DOS at high concentrations nor split-off

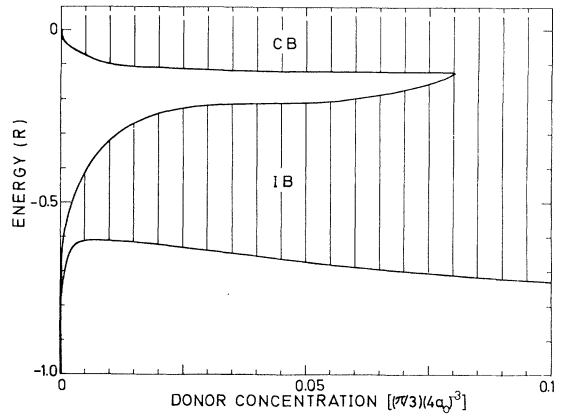

FIG. 2. Energies of conduction-band (CB) and impurity-band (IB) edges as functions of donor concentrations.

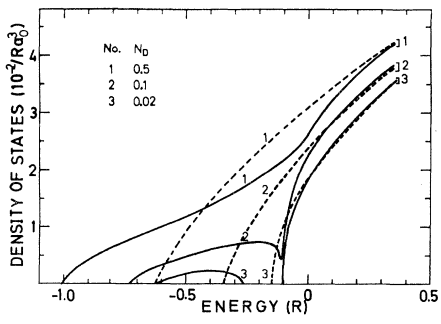

FIG. 3. DOS's for three typical concentrations in the present approximation (full lines) and in the high-density approximation (dashed lines).

IB at low concentrations; finally, the DOS is less extended towards low energies than in the present approximation.

VI. SPECTRAL DENSITY AND LOCALIZATION STUDIES

Let us recall that our multiple-scattering method leads to a wave-vector-dependent self-energy $\Sigma(\vec{k},E)$ [Eq. (2c)]. It follows that the study of the spectral density $A(\vec{k},E)$ [Eq. (3)] which is the average probability that an electron having energy E is in the state $|\vec{k}\rangle$, may bring further information on the electronic structure of our system.

Curves of Fig. 4 show for three typical donor concentrations the variation of $A(\vec{k},E)$ as a function of k at different energies. At low enough concentrations (e.g., $N_D=5\times10^{-3}$, in Fig. 4) for which a split-off IB exists, $A(\vec{k},E)$ exhibits two kinds of behavior: in the CB ($E=0$), it has a narrow Lorentzian shape with a peak at $k\neq0$ while in the IB ($E=-0.5$) it presents a broad maximum at $k=0$ and extends widely in the k space. The former behavior is what is to be expected for a quasifree electron. The most probable wave vector is that of the maximum of $A(\vec{k},E)$ and the narrow width Δk shows through the uncertainty relation $\Delta\vec{k}\cdot\Delta\vec{r}=\text{const}$ that the corresponding state is indeed extended in real space. In contrast, the latter behavior is typical for a localized state (the most probable wave vectors are centered at $k=0$ and the width Δk is large). At the concentration for which the IB just touches to the CB ($N_D=0.08$, Fig. 4) the spectral densities in the IB ($E=-0.15$) and in the body of CB ($E=+0.25$) have, respectively, the same shape as above. However, in the CB but near its edge ($E=-0.05$), it shows an intermediate shape: $A(\vec{k},E)$ is finite at $k=0$, has a broad peak at $k\neq0$, and is asymmetric. This shape may be interpreted as a result of hybridization between localized and extended states. For higher concentrations (e.g., $N_D=0.5$, Fig. 4) for which there is no gap in the DOS, one still observes the three kinds of behavior described above. Thus starting from the band edge one finds successively localized, hybrid, and extended states as energy increases. The degree of localization may be estimated by the ratio $R=A(k=0,E)/A(k_m,E)$ where k_m is the value of k for which $A(k,E)$ is maximum. Domains of existence of the various kinds of states are displayed in Fig. 1. Region I is the domain of localized states, i.e., corresponding to energies for which the ratio $R=1$. For higher energies, R varies continuously from one to zero. The shape of this variation (which resembles a finite-temperature Fermi-Dirac distribution function) suggests that one can distinguish between two regions: region II for which $R\gtrsim10\%$, corresponds mainly to hybrid states and region III ($R\lesssim10\%$) corresponds to extended states. As can be seen in Fig. 1, region II, which does not exist when a DOS gap exists, widens out as N_D increases.

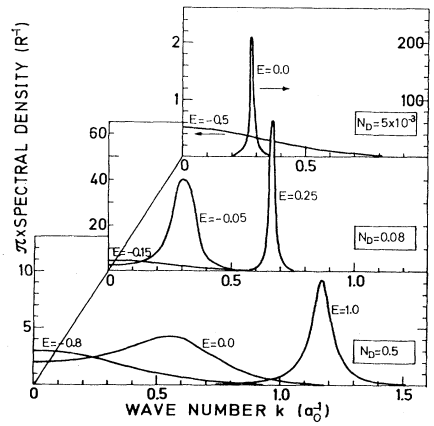

FIG. 4. Comparison of the spectral densities $A(\vec{k},E)$ (times π) as functions of k at typical energies and for three typical concentrations.

This discussion of localization which is based on the spectral density-shape analysis has certainly to be confirmed by calculations of ensemble-averaged wave-function extension as a function of energy and also by mobility calculations which require the knowledge of a two-particle Green function.

In order to calculate the Fermi level, one has to ask the question of spin degeneracy. As in our model, the interaction potential does not depend explicitly on spin, it is necessary to make assumptions on this degeneracy. For low concentrations with a split-off IB, we assume, as it is likely the case, that an impurity binds only one electron so that the IB is full at zero temperature. Consequently the IB's DOS's in Fig. 1 must be divided by a factor of 2 [cf. the text after Eq. (4)]. In contrast, the CB states which are quasifree should be spin degenerate (region III in Fig. 1). For concentrations with no gap we assume that electron states of region I (Fig. 1) which have identical spectral density to those of IB's, are not spin degenerate. It should be reasonable to assume that in region II, the spin-degeneracy factor varies continuously from one to two as energy increases. If this variation of spin degeneracy with energy is accounted for, the band-tail DOS in Fig. 1 should be modified accordingly. In keeping with the above considerations, it is found that when no gap appears the Fermi level lies approximately near the boundary between regions II and III. It should be noted that for concentrations slightly higher than that for which the IB just merges with the CB, the spectral density at Fermi level $A(k,E_F)$ still shows a broad peak in k space. This means that the average charge density around an impurity is far from being uniform.

The pseudodispersion curves are plotted in Fig. 5 for two concentrations with and without gap, respectively. This is achieved by associating with every energy E the most probable wave number k_m. The values k_+ and k_- defined by $A(k,E)=\frac{1}{2}A(k_m,E)$ allow one to estimate the broadening $\Delta k=k_+-k_-$. As can be seen, this broadening decreases as energy increases in the CB, as a result of weaker scattering. It should be noted that the broadenings in region I for both concentrations are comparable. In conclusion, it is important to note that even if there is no DOS gap, a non-negligible fraction of electrons is localized.

VII. COMPENSATION EFFECTS

In this section the compensation effects on both CB and VB electronic structures within the effective-mass approx-

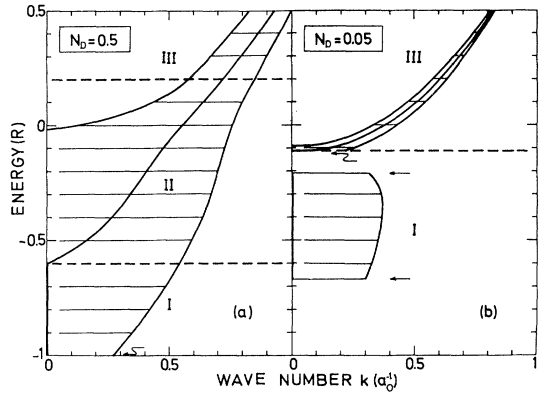

FIG. 5. Pseudodispersion curves for (a) a DOS without gap ($N_D=0.5$); (b) a DOS with a gap ($N_D=0.05$). Regions I, II, and III delimited by dashed lines are those defined in Fig. 1. Hatched areas represent the broadening Δk of the spectral density (see text). The locus of the most probable wave number k is represented by the full line inside these areas in regions II and III and by the full line $k=0$ in region I. The band edges are indicated by arrows.

imation are studied. Our system is now characterized by the concentrations N_D and N_A of donors and acceptors, respectively. At given donor concentration N_D, as the compensation ratio $K=N_A/N_D$ is increased several effects may be qualitatively predicted: The total concentration of scattering centers increases; the impurity potential becomes less screened because the carrier concentration $N=N_D-N_A$ decreases; finally the Fermi level is lowered so that it may be in the lower part of the band tail where the states are localized.

We have first considered an uncompensated system with a concentration N_D such that the (negative) potential is strong enough to form a split-off IB near the bottom of CB. We have changed the potential sign. As expected, no IB appears in this energy range and the CB's DOS remains practically unchanged. Changing the sign of the potential amounts to describing the effect of donors (acceptors) on VB's (CB) assumed to have the same effective mass. This effect is thus negligible for such a concentration. However, for higher concentrations ($N_D>1$), a tail appears at the top of the VB and extends more and more into the gap as N_D increases. This effect can be easily understood: The second-order term in interaction, which results in both VB's and CB's extending inside the gap, becomes the leading term at high concentrations. However, at usual high doping levels, the VB-tail extension is smaller than that of the CB tail. For instance, at $N_D=10$, the latter amounts to $2.5R$ whereas the former amounts to only $0.65R$.

In order to describe CB electronic states in a compensated system, the multiple-scattering equations [Eqs. (8a)–(8d)] may be generalized as follows:

$$U_D(\vec{k},\vec{q};E)=-N_D\,|\,v(\vec{k}-\vec{q})\,| - \frac{1}{(2\pi)^3}\int d^3q'\,|\,v(\vec{q}'-\vec{q})\,|\,G(\vec{q}') \times U_D(\vec{k},\vec{q}';E)\,, \tag{10a}$$

$$U_A(\vec{k},\vec{q};E)=+N_A\,|\,v(\vec{k}-\vec{q})\,| + \frac{1}{(2\pi)^3}\int d^3q'\,|\,v(\vec{q}'-\vec{q})\,|\,G(\vec{q}') \times U_A(\vec{k},\vec{q};E)\,, \tag{10b}$$

$$\Sigma_D(\vec{k},E)\equiv U_D(\vec{k},\vec{k};E)+N_D\,|\,v(0)\,|\,, \tag{10c}$$

$$\Sigma_A(\vec{k},E)\equiv U_A(\vec{k},\vec{k};E)-N_A\,|\,v(0)\,|\,, \tag{10d}$$

$$\Sigma_{ei}(\vec{k},E)=\Sigma_D(\vec{k},E)+\Sigma_A(\vec{k},E)\,, \tag{10e}$$

$$\Sigma(\vec{k},E)=\Sigma_{ei}(\vec{k},E)+\Sigma_{xc}(\vec{k},E)\,, \tag{10f}$$

$$G(\vec{k},E)=[E-\epsilon_k-\Sigma(\vec{k},E)]^{-1}\,. \tag{10g}$$

The subscripts D and A in Eqs. (10a)–(10e) refer to donors and acceptors, respectively. Equation (10e) defining the electron-impurity interaction self-energy Σ_{ei} is depicted by the sum of two series of diagrams similar to that of Fig. 9 in Appendix A, one for donors and the other for acceptors. As before, because of electrical neutrality, there is no first-order Coulomb term in the interaction. Equations (10a) and (10b) are coupled nonlinear integral equations through the perturbed Green function G which depends on both U_D and U_A [see Eqs. (10c)–(10g)]. This involves the inclusion among others of diagrams such as that illustrated by Fig. (9d) in which impurities i and j are now two donors, or one donor and one acceptor, or two acceptors. Crossed diagrams such as that of Fig. 9(e) are excluded. As before (see Sec. III), this is a single-site approximation and neglects any correlation between impurities.

To describe VB electronic states, it suffices to exchange N_D and N_A in Eqs. (10a)–(10g) and to invert the energy axis. The physical quantities are then expressed in the reduced units appropriate to VB's. It should be noted that in n- (p-) type systems, the exchange-correlation contribution to the self-energy in Eq. (10f) is negligible for VB (CB) states.

We have solved the set of equations (10a)–(10g) in exactly the same way as described in Sec. IV, for different donor concentrations N_D and for different compensation ratios K.

We have considered the question of whether the compensation which reduces the carrier concentration and thus the screening effects, would lead to the opening of the gap. To this end, we have solved Eqs. (10a)–(10g) at the onset of the IB splitting (i.e., at $N_D=0.1$) for different compensation ratios. The results are shown in Fig. 6. As can be seen, no gap opens even at $K=0.99$ but one observes a stretching of IB toward low energies, this being more pronounced the higher the compensation. It has been checked that the integrated DOS over the IB is equal to N_D whatever the compensation. To single out the respective effects of potential strength and of the presence of acceptors, we have kept the screening length constant and varied the compensation ratio. The donor band is then pushed towards high energies (over about $0.2R$ for $K=0.99$). Therefore, the two effects are opposite as could be anticipated qualitatively.

The curves in Fig. 7 depict the effects of compensation in a more doped system ($N_D=2$). Here again one observes

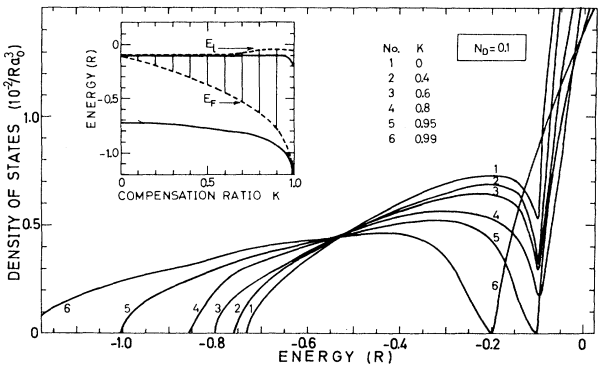

FIG. 6. Evolution of the DOS when the compensation ratio K is increased in the case where the IB just merges with the CB ($N_D=0.1$). The inset shows the energies of band edges (full lines), the Fermi level E_F, and the boundary E_I between regions I and II (dashed lines) as functions of the compensation ratio.

a stretching of the band tail towards low energies which increases with compensation. It is clear that while the band tail (or the IB at lower concentrations) is emptied of its electrons, its DOS becomes more distorted (see Figs. 6 and 7). Therefore, the rigid-band model is not appropriate here.

In order to study the compensation effects on VB's, the CB-to-VB mass ratio m_c/m_v has to be considered. We have confined ourselves to the study of two typical cases: $m_v=m_c$ and $m_v=10m_c$. Within the effective-mass approximation, the former would correspond approximately to germanium and silicon and the latter to gallium arsenide. In Fig. 8, the CB and VB DOS's are plotted for $N_D=0.1$ and $K=0.4$ and for the two mass ratios. For $m_v=m_c$, the relevant reduced units of the VB are those of the CB. The VB's DOS (Fig. 8) may then be compared with that of curve 7 in Fig. 1 ($N_D=0.05$) which shows a gap of $0.1R$. Indeed, both systems have nearly the same carrier concentration. In the compensated case, an IB does exist (the integrated DOS of which is equal to N_A) but it is right against the VB. Hence donors act on the acceptor band in the same way as acceptors on the donor band. As for the case $m_v=10m_c$, the concentrations ex-

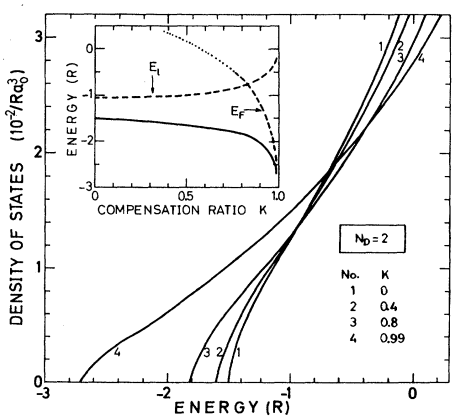

FIG. 7. Same as Fig. 6 except that here there is a single band with a tail ($N_D=2$).

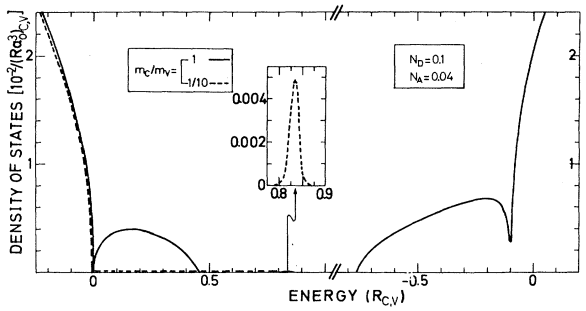

FIG. 8. DOS's of conduction, valence, donor, and acceptor bands of a compensated system with $N_D=0.1$ and $K=0.4$ for two CB-to-VB mass ratios: $m_c/m_v=1$, full lines; $m_c/m_v=\frac{1}{10}$, dashed lines. CB and donor-band DOS's are practically the same in both cases. Zero energy is taken at the bottom (top) of the unperturbed CB (VB).

pressed in the VB units are now $N_D=10^{-4}$ and $N_A=4\times10^{-5}$. The corresponding VB's DOS (Fig. 8) should then be compared with that of curve 12 in Fig. 1 ($N_D=5\times10^{-5}$). The DOS's are similar but, as previously, under the effects of donors the IB shifts (slightly) towards the VB.

From spectral density studies, for every value of N_D and of K, one may calculate the energy E_I below which electrons are localized (i.e., the upper limit of region I defined in Sec. VI). In the insets of Figs. 6 and 7 the energy E_I, the Fermi level E_F, and the band edges are plotted as functions of compensation ratio K. In both cases, as the latter increases, the Fermi level is lowered and descends well into the energy range where electron states are localized. Therefore, it seems clear that an activation energy should be necessary to promote electrons in the energy range where the mobility should be higher.

VIII. DISCUSSION OF THE RESULTS AND COMPARISON WITH EXPERIMENT

It turns out that the experimental critical concentration N_c for the M-NMT (Ref. 1) in various doped semiconductors with quasihydrogenic impurities is in most cases very close to that given by the Mott criterion[27]: $N_c^{1/3}a_0\simeq0.25$ (a_0 is the effective Bohr radius of the isolated impurity).

If one assumes the observed activation energy in conductivity experiments to be due to an energy gap between IB and CB, the critical concentration which corresponds in our calculations to the closing of the gap ($N_D^{1/3}a_0\simeq0.12$) is about 10 times smaller than observed experimentally. This discrepancy ought to be ascribed to the lack of multiple-occupancy corrections (see discussion in Sec. III). We believe, however, that it is likely to be due to the use of TF potential which, as is well known, is overscreened[28] at usual concentrations and deviates markedly from the true potential which may be reached by self-consistent calculations.[29] To verify this assertion, we have arbitrarily enhanced the TF potential by multiplying it by a constant, and alternatively by increasing the screening length. In both cases, the gap closes up at higher concentrations. For example, if the potential is twice as strong, a gap of $0.2R$ opens between an IB and CB for $N_D=1$ (i.e., $N_D=N_C$ in usual units).

Within the TF approximation for the potential, the Fermi level for uncompensated systems lies either in the gap between IB's and CB's at low concentrations or almost within the extended states' energy range when no gap appears. However, the situation may be quite different if the potential range is increased. For example, for $N_D=1$, if the screening length is doubled, there is still no gap but the Fermi level is now in the intermediate region (region II) very close to the localized states' energy range. In this case, according to our discussion of localization (see Sec. VI), an activation energy would be needed to promote electrons to a higher mobility energy range. On these grounds, one cannot ascertain whether the M-NMT occurs at the closing of a DOS gap or once the Fermi level enters an energy range within a continuum, where states are mobile enough. The above example clearly shows that conclusions concerning the nature of the transition depend on the model potential. A definite answer to this question necessarily presupposes the use of a completely self-consistent, spin-dependent potential. Moreover, such a potential would enable us to see whether the D^- band (as defined within the Mott-Hubbard scheme[30]) exists or not and if it exists[31] how it merges with the IB (D^0 band) and CB in the M-NMT range.

Let us now discuss how our results compare with some experimental data. Theoretical analyses[32] of differential conductivity in DSC-metal tunnel junctions may, with some simplifying assumptions, lead to the DOS of DSC around the CB (VB) edge. Such DOS's have been experimentally obtained in various n- and p-type semiconductors at impurity concentrations close or higher than N_C.[33] Although the concentration for which the IB just merges with the CB is in our calculations an order of magnitude lower than the experimental value (see discussion above), it is noteworthy that the shapes of calculated DOS's (Fig. 1) closely resemble those of experimental ones. However, the experimental band tail is somewhat more extended in the gap than that calculated. This may be ascribed at least partly to statistical concentration fluctuations which are omitted here (see Sec. II).

It is well established that heavily DSC's show a substantial gap shrinkage.[34] This phenomenon has particularly been studied in p-type gallium arsenide especially by photoluminescent experiments.[35] It is generally admitted that the gap shrinkage ΔE_g approximately obeys a one-third power law in concentration $\Delta E_g \simeq -CN_D^{1/3}$ ($N_A^{1/3}$). The experimental values of the constant C obtained[35] for p-type gallium arsenide lie between 1.6 and 2.4×10^{-8} eV cm. Our model is well suited to the calculation of the gap shrinkage in the relevant concentration range ($N_D, N_A > 1$). The shrinkage arises from both CB and VB shifts inside the gap. However, in the case of gallium arsenide, the VB effective mass is about 10 times larger than the CB one so that for a given (high) acceptor concentration the shift of the CB is negligible compared to that of the VB (see Sec. VII). The shift of VB (CB) results from two contributions of comparable importance: the exchange-correlation term and the electron-impurity interaction term. Our calculations lead to a total band-edge shift approximately obeying a $N_A^{1/3}$ law: $\Delta E_g \simeq -1.2N_A^{1/3}$ in reduced units. When applied to the case of p-type gallium arsenide these calculations lead to the gap shrinkage ΔE_g (eV) $=-2.5\times10^{-8}N_A^{1/3}$ (cm^{-1}) with standard values for effective mass and dielectric constant. As in the concentration range of interest the use of the TF potential is fully justified, the agreement between theory and experiment is not surprising. The above conclusions are valid to the extent that the VB effective mass is large enough compared to that of the CB. If the two masses are comparable, one has to account for the shifts of both bands. Practically speaking, consider an uncompensated n-type DSC with equal VB and CB effective masses. This should be approximately the case of n-type silicon or n-type germanium. It is found that the gap shrinkage in reduced units is given by the relation $\Delta E_g \simeq -1.2N_D^{1/3} - 0.18N_D^{0.55}$. The first term is the same as before while the second term describes VB shift.[36] It should be noted that in the high-density approximation (see Sec. V) in which the electron-impurity potential sign plays no role, both terms in the above relation should be equal. In the present approximation, although the tail extension of the VB is smaller than that of the CB in the concentration range of interest, it should be remarked that the VB tail DOS is approximately twice as large as that of the CB starting from respective band edges.

Various experiments[1,3,37] have clearly shown that the physical properties of semiconductors around the critical concentration for M-NMT cannot be merely interpreted with simple models either of bound states on the insulating side or of free states on the metallic side. Our method is well suited, despite certain imperfections, to the study of electronic structure of DSC's at all usual impurity concentrations. It allows one in principle to calculate quantities such as specific heat and magnetic susceptibility in particular in the vicinity of M-NMT. However, the results which would be obtained with a not completely self-consistent scattering potential (present model) would have to depend heavily on that potential, and could not validly be confronted with experiment. Nonetheless one may within the present model propose a qualitative interpretation of the observed behavior of electronic specific heat in the vicinity of M-NMT. An electronic specific heat depending linearly on temperature, $C_e=\gamma T$, has been observed experimentally[37] in phosphorus-doped silicon for concentrations below the critical value for M-NMT over at least half an order of magnitude. If the coefficient γ in the above relation is assumed to be essentially proportional to the DOS at Fermi level, then one must admit that the Fermi level lies in a continuum of localized states in that concentration range. Under these conditions, the activation energy observed in conductivity experiments in the same concentration range may be interpreted as the average energy needed to promote some localized electrons lying near the Fermi level to higher energies for which the mobility is higher. No such situation is found for uncompensated systems in our model as it is. However, it may occur for compensated systems or when the TF potential range is arbitrarily increased.

Electrical conductivity in highly doped, compensated, n-type germanium samples[38] ($N_D \simeq 10$–50) for a given N_D shows an activation energy which increases with increasing compensation. These results may be interpreted in our model as follows: As the compensation ratio is increased, the Fermi level is lowered so that it penetrates well into the localized states' energy range (see Figs. 6 and 7). This interpretation seems to be supported by the fact that the

Hall mobility at helium temperature[38] decreases over 3 orders of magnitude but continuously as the compensation increases.

IX. CONCLUSION

We have used a multiple-scattering method to calculate the electronic structure of doped (and compensated) semiconductors in a large impurity concentration range. We have shown how the band tail is transformed into a split-off impurity band below a certain concentration. The ability of this method to include a realistic impurity potential and electron correlation effects, allows us to give a description of electronic properties of these systems in reasonable agreement with experiment.

Spectral density analysis allows one to distinguish between localized and extended states and provides elements for a discussion of localization and its connection with the nature of metal-nonmetal transition. However, a definite answer to this question will undoubtedly involve the inclusion of a completely self-consistent, spin-dependent scattering potential in the theory and the corresponding mobility calculations.

ACKNOWLEDGMENTS

We would like to express our thanks to P. Leroux-Hugon and B. Roulet for a number of stimulating conversations.

APPENDIX A: DERIVATION OF KLAUDER'S MULTIPLE-SCATTERING THEORY

This derivation is achieved diagrammatically in three stages.

(i) In the first stage, one extracts from all scattering processes those occurring on a single impurity and then performs the sum over impurities. The average value over all possible positions of impurities of the electron propagator is calculated in the Kohn-Luttinger sense,[11] the impurities being considered as independent. This leads to the following self-energy:

$$\Sigma_{ei}(\vec{k},E)=\frac{N_D}{(2\pi)^3}\int d^3q' v(\vec{q}')G_0(\vec{k}+\vec{q}')v(-\vec{q}')$$
$$+\frac{N_D}{(2\pi)^6}\int d^3q' d^3q'' v(\vec{q}')G_0(\vec{k}+\vec{q}')v(\vec{q}''-\vec{q}')G_0(\vec{k}+\vec{q}'')v(-\vec{q}'')+\cdots$$
$$=N_D\sum_{p=1}^{\infty}\frac{1}{(2\pi)^{3p}}\int d^3q' d^3q''\cdots d^3q^{(p)}v(\vec{q}')G_0(\vec{k}+\vec{q}')v(\vec{q}''-\vec{q}')\cdots G_0(\vec{k}+\vec{q}^{(p)})v(-\vec{q}^{(p)}) , \tag{A1}$$

where $G_0=(E-\epsilon_k+i0)^{-1}$ is the unperturbed Green function. It should be noted that in Eq. (A1) no linear term in v appears (see Sec. II). $\Sigma_{ei}(k,E)$ thus determined is represented diagrammatically by Fig. 9(a). It is easy to see that the series expansion in Eq. (A1) may be put in compact form by introducing the vertex function K defined by the following integral equation:

$$K(\vec{k},\vec{q};E)=\frac{1}{(2\pi)^3}\int d^3q' v(\vec{q}'-\vec{q})G_0(\vec{k}+\vec{q}')[N_D v(-\vec{q}')+K(\vec{k},\vec{q}';E)] . \tag{A2a}$$

It is clear that

$$\Sigma_{ei}(\vec{k},E)\equiv K(\vec{k},\vec{q}=0;E) , \tag{A2b}$$

as can be seen by iterating Eq. (A2a) over K.

(ii) If one accounts for all scattering processes on all impurities contributing to the self-energy, besides the linear terms in Eq. (A1) one has to add terms in N_D^2, N_D^3, etc. For instance, the contribution to $\Sigma_{ei}(\vec{k},E)$ of the scattering process sketched in Fig. 9(f) is a term in $N_D^2 v^4$. One approximate way to account for such processes is to perform a summation of the corresponding diagrams. This is achieved with the help of the Dyson equation which involves a series expansion in powers of Σ:

$$G(\vec{k},E)=G_0(\vec{k},E)+G_0(\vec{k},E)\Sigma(\vec{k},E)G(\vec{k},E)$$
$$=[G_0^{-1}(\vec{k},E)-\Sigma(\vec{k},E)]^{-1} . \tag{A3}$$

This equation is illustrated by Fig. 9(b) and corresponds to the fourth Klauder's approximation[4] [Eqs. (69)—(71) of his paper]. Σ is the total self-energy defined in Eq. (2c).

(iii) Now if the bare propagator G_0 is replaced by the dressed propagator G in the expression of Σ_{ei} in Eq. (A1) or in the expression of K in Eq. (A2a) [this amounts to substituting the series of Fig. 9(a) by that of Fig. 9(c)] a new class of diagrams is then incorporated. An example of these diagrams is represented by Fig. 9(d) which clearly shows that an electron being scattered by an impurity has been scattered by all other impurities; in other words it propagates in an effective medium. This corresponds to the Klauder's fifth approximation which is expressed by Eqs. (2a)—(2d).

In Sec. V we will compare this approximation to that effective-medium approximation in which the scattering on a given site is treated to second order only. The latter is the third Klauder's approximation [Eqs. (62) and (63) of his paper]. In this case Σ_{ei} is given by the first term of the sum illustrated by Fig. 9(c) only. It is expressed by the set of Eqs. (2a)—(2d) with $K=0$ in the right-hand member of Eq. (2a). This is a high-density approximation because it includes terms in $N_D^p v^{2p}$ with $p=2,3,\ldots$ [see Figs. 9(f) and 9(g)] but neglects terms in $N_D v^{2p}$ [Fig. 9(h)]. Moreover it is also a weak scattering approximation because in

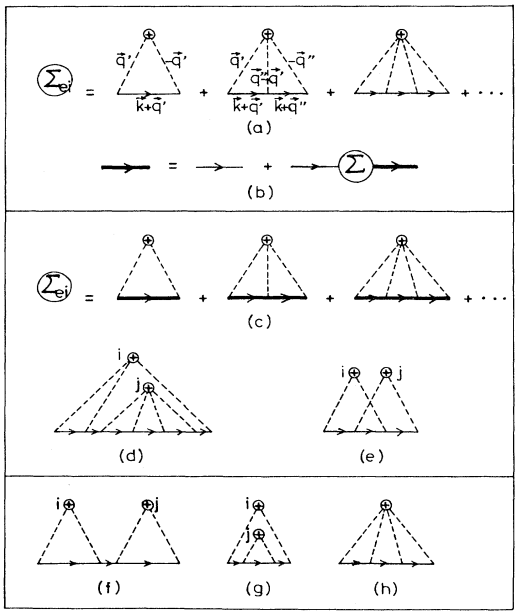

FIG. 9. Electron-impurity self-energy diagrams involved in various approximations (see text). Interaction lines are dashed. Thin and thick full oriented lines represent the bare and the dressed propagators, respectively. Crosses inside small circles represent impurities and carry a factor N_D.

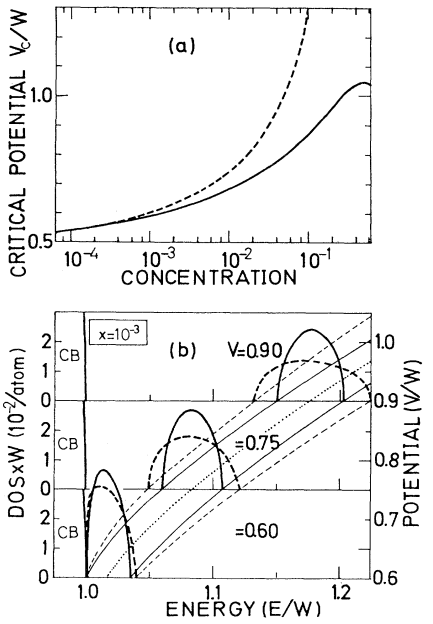

FIG. 10. Comparison of the CPA (full lines) and the KA (dashed lines) for a model of δ-function impurity potential and host-matrix semielliptic DOS the half-bandwidth of which is taken as unit of energy: (a) Critical potential for CB-IB splitting as a function of concentration x (semilogarithmic scale). (b) For $x=10^{-3}$, CB-edge and IB DOS's (left scale) as functions of energy for three values of potential, $V=0.60$, 0.75, and 0.90; the energies of the IB edges and of the Koster-Slater model (dotted line) are also plotted as functions of potential strength (right scale).

Σ_{ei} terms in $v^3, v^4, \ldots$ are neglected. This is the reason why this approximation is valid only at high energies.

The third, fourth, and fifth Klauder's approximations described above are single-site approximations because in stage (i) the averaging process has been performed assuming that all impurity positions are equiprobable and that there are no correlations between sites, and in stage (ii) the partial summation operation does not include scattering processes such as that illustrated by the crossed diagram of Fig. 9(e).

APPENDIX B: MULTIPLE-OCCUPANCY CORRECTION EFFECTS

The purpose of this appendix is to study quantitatively the effects of multiple-occupancy corrections on the DOS of a binary-alloy model. It should be noted that DSC's with substitutional impurities (e.g., phosphorus-doped silicon) are in fact very dilute binary alloys with concentration x (i.e., the ratio of the number of impurities to the total number of atoms) of the order of 10^{-6} to 10^{-4}. In the framework of the tight-binding model with a δ-function potential, the expressions of electronic self-energy with corrections, i.e., in CPA, and without corrections, i.e., in Klauder's approximation (KA) read, respectively[6]:

$$\Sigma_c = \frac{xV}{1-(V-\Sigma_c)F(E-\Sigma_c)} , \tag{B1}$$

$$\Sigma_K = \frac{xV}{1-VF(E-\Sigma_K)} , \tag{B2}$$

where V is the impurity potential and

$$F(z) = \int \frac{D(E)}{z-E} dE . \tag{B3}$$

Here $D(E)$ is the DOS per atom and per unit energy. For an unperturbed semielliptic band centered at zero energy with a half-width W, we have[39]

$$D_0(E) = \left[\frac{2}{\pi W^2}\right](W^2-E^2)^{1/2} , \quad |E| \le W . \tag{B4}$$

Then

$$F(z) = \left[\frac{2}{W^2}\right][z-(z^2-W^2)^{1/2}] . \tag{B5}$$

The DOS of the alloy is

$$D(E) = -\left[\frac{1}{\pi}\right]\mathrm{Im}F(E+i0) . \tag{B6}$$

Both CPA and KA lead to a cubic equation either for Σ or for F. As its coefficients are real, this equation may have either three real roots or one real root and two complex conjugate roots. According to Eq. (B6) it is clear that the DOS is nonzero only for the latter case. Band edges are obtained under the condition that the above cubic equation has a double root. At given concentration and potential strength, the band-edge energies are then the real solutions of a quartic equation which may have either two or four real roots. The former case corresponds to a single band, and the latter to an IB split off from the main band.

The DOS has been calculated numerically for different values of x and of V within the bands thus determined, using the formula (B6) and taking the appropriate solution of the equation obeyed by F.

The results are illustrated in Fig. 10. As can be seen, the critical potential V_c for the opening of the gap [Fig. 10(a)] is practically the same in the CPA and KA for concentrations typically lower than 1%. At higher concentrations, the multiple-occupancy corrections cannot be neglected. For a low concentration ($x=10^{-3}$) we have plotted in Fig. 10(b) the DOS per atom of the IB and of the CB edge in the CPA and in the KA at three values of the potential (taken positive here) high enough to open a gap. The positions of IB edges as functions of potential strength are plotted in the same figure in both approximations. As can be seen, the IB is somewhat wider in the KA than in the CPA. This is a general feature. Finally, it is worth noting that in both approximations and for low concentrations [see Fig. 10(b)] the IB is centered on the value given by the Koster-Slater (KS) model in the very dilute limit: $E_{KS}=(W^2+4V^2)/4V$; this formula is obtained by the well-known condition $VF=1$.

[1]For a recent review of experimental and theoretical works, see *The Metal Non-Metal Transition in Disordered Systems,* edited by L. R. Friedman and D. P. Tunstall (SUSSP Publications, Edinburgh, 1978). See also Philos. Mag. B 42, 723 (1980).

[2]For a recent review, see *Anderson Localization,* Vol. 39 of *Springer Series in Solid-State Sciences,* edited by Y. Nagaoka and H. Fukuyama (Springer, Berlin, 1982).

[3]H. F. Hess, K. DeConde, T. F. Rosenbaum, and G. A. Thomas, Phys. Rev. B 25, 5578 (1982); M. A. Paalanen, T. F. Rosenbaum, G. A. Thomas, and R. N. Bhatt, Phys. Rev. Lett. 48, 1284 (1982); G. A. Thomas, A. Kawabata, Y. Ootuka, S. Katsumoto, S. Kobayashi, and W. Sasaki, Phys. Rev. B 26, 2113 (1982).

[4]J. R. Klauder, Ann. Phys. (N.Y.) 14, 43 (1961).

[5]T. Matsubara and Y. Toyozawa, Prog. Theor. Phys. 26, 739 (1961).

[6]F. Yonezawa and K. Morigaki, Prog. Theor. Phys. 53, 1 (1973); R. J. Elliott, J. A. Krumhansl, and P. L. Leath, Rev. Mod. Phys. 46, 465 (1974).

[7]We thank B. Roulet for drawing our attention to the multiple-occupancy corrections.

[8]A. Ghazali and J. Serre, Phys. Rev. Lett. 48, 886 (1982); A. Ghazali and J. Serre, in Proceedings of the 16th International Conference on the Physics of Semiconductors, Montpellier, France, 1982 [Physica B 117&118, 84 (1983)].

[9]J. Serre, A. Ghazali, and P. Leroux-Hugon, Phys. Rev. B 23, 1971 (1981).

[10]See, e.g., A. L. Fetter and J. D. Walecka, *Quantum Theory of Many-Particle Systems* (McGraw-Hill, New York, 1971), p. 64.

[11]W. Kohn and J. M. Luttinger, Phys. Rev. 108, 590 (1957), Appendix B.

[12]P. A. Wolff, Phys. Rev. 126, 405 (1962).

[13]L. Hedin and B. I. Lundqvist, J. Phys. C 4, 2064 (1971).

[14]O. Gunnarsson and B. I. Lundqvist, Phys. Rev. B 13, 4274 (1976).

[15]L. Hedin, Phys. Rev. 139, A796, (1965); L. Hedin and S. Lundqvist, J. Phys. (Paris) 33, C3-73 (1972); B. Winter, Phys. Rev. B 17, 2429 (1978).

[16]See, e.g., D. Pines, *Elementary Excitations in Solids* (Benjamin, New York, 1963), p. 146.

[17]See, e.g., P. Leroux-Hugon and A. Ghazali, Phys.Rev. B 14, 602 (1976).

[18]W. Kohn and L. J. Sham, Phys. Rev. 140, A1133 (1965).

[19]F. Yonezawa, Prog. Theor. Phys. 31, 357 (1964).

[20]Similar discussions can be found in the studies of the Newmann series expansion of integral equations; see, e.g., R. Courant and D. Hilbert, *Methods of Mathematical Physics* (Interscience, New York, 1966).

[21]See, e.g., N. Minorsky, in *The Mathematics of Physics and Chemistry,* edited by H. Margenau and G. M. Murphy (Van Nostrand, Princeton, New Jersey, 1964), Vol. II, p. 321; G. H. Pimbley, Jr., *Eigenfunction Branches of Nonlinear Operators, and Their Bifurcations* (Springer, Berlin, 1969); G. Iooss and D. J. Joseph, *Elementary Stability and Bifurcation Theory* (Springer, New York, 1980).

[22]The chosen concentration unit is equal to the Mott's critical concentration N_c given by $N_c^{1/3}a_0\simeq 0.25$.

[23]J.-P. Gaspard and F. Cyrot-Lackmann, J. Phys. C 6, 3077 (1973).

[24]See, e.g., H. Nakanishi, F. Yonezawa, and T. Matsubara, Solid State Commun. 40, 15 (1981), and references therein.

[25]See, e.g., H. Ehrenreich and L. M. Schwartz, in *Solid State Physics,* edited by H. Ehrenreich, F. Seitz, and D. Turnbull (Academic, New York, 1976), Vol. 31, Sec. II.

[26]According to our choice of reduced units, the integrated DOS has to be multiplied by $192/\pi$ in order to obtain N_D.

[27]N. F. Mott, Philos. Mag. 6, 287 (1961).

[28]J. B. Krieger and M. Nightingale, Phys. Rev. B 4, 1266 (1971).

[29]See, e.g., C. O. Almbladh, U. von Barth, Z. D. Popović, and M. J. Stott, Phys. Rev. B 14, 2250 (1976).

[30]N. F. Mott, Adv. Phys. 21, 785 (1972).

[31]For a quantitative study of the Mott-Hubbard model see, e.g., R. Riklund and K. A. Chao, Phys. Rev. B 26, 2168 (1982).

[32]G. D. Mahan and J. W. Conley, Appl. Phys. Lett. 11, 29 (1967); N. Sawaki and T. Arizumi, J. Phys. Soc. Jpn. 35, 684 (1973).

[33]N. Sawaki, A. Yoshida, and T. Arizumi, J. Phys. Soc. Jpn. 36, 149 (1974); K. P. Abdurakhmanov, Sh. Mirakhmedov, A. Teshabaev, and S. S. Khudaĭberdiev, Fiz. Tekh. Poluprovodn. 10, 658 (1976) [Sov. Phys.—Semiconduc. 10, 393 (1976)].

[34]For a review, see R. A. Abram, G. J. Rees, and B. L. H. Wilson, Adv. Phys. 27, 799 (1978).

[35]H. C. Casey, Jr. and F. Stern, J. Appl. Phys. 47, 631 (1976); D. Olego and M. Cardona, Phys. Rev. B 22, 886 (1980); A. N. Titkov, E. I. Chaĭkina, E. M. Komova, and N. G. Ermakova, Fiz. Tekh. Poluprovodn. 15, 345 (1981) [Sov. Phys.—Semiconduc. 15, 198 (1981)].

[36]It can be noted that the observed gap shrinkage in highly doped n-type silicon obeys approximately a $N_D^{1/2}$, rather than $N_D^{1/3}$ law; see M. Balkanski, A. Aziza, and E. Amzallag, Phys. Status Solidi 31, 323 (1969). Besides, intervalley scattering seems to be important in this case; see A. Selloni and S. T. Pantelides, Phys. Rev. Lett. 49, 586 (1982).

[37]N. Kobayashi, S. Ikehata, S. Kobayashi, and W. Sasaki, Solid State Commun. 24, 67 (1977); 32, 1147 (1979); G. A. Thomas, Y. Ootuka, S. Kobayashi, and W. Sasaki, Phys. Rev. B 24, 4886 (1981).

[38]W. Sasaki and C. Yamanouchi, J. Non-Cryst. Solids 4, 183 (1970).

[39]B. Velický, S. Kirkpatrick, and H. Ehrenreich, Phys. Rev. 175, 747 (1968).